Effect of TiO2 Nano-filler on Electrical Properties of Na+ Ion Conducting PEO/PVDF Based Blended Polymer Electrolyte

Kiran Kumar Ganta
Department of Physics, B V Raju Institute of Technology, Narsapur, Medak, Telangana 502313, India.
Venkata Ramana Jeedi
Department of Physics, B V Raju Institute of Technology, Narsapur, Medak, Telangana 502313, India.
K. Vijaya Kumar
Department of Physics, JNTU Hyderabad, Kukatpally, Hyderabad, Telangana 500085, India.
Yalla Mallaiah
Department of Physics, University PG College, Secunderabad, Osmania University, Hyderabad, Telangana 500003, India
E. Laxmi Narsaiah (laxminarsaiah.emmadi@bvrit.ac.in)
Department of Physics, B V Raju Institute of Technology, Narsapur, Medak, Telangana 502313, India.
https://orcid.org/0000-0001-9257-0067

Research Article

Keywords: TiO2 Nano-filler, Electrochemical Impedance Spectroscopy, Ionic conductivity, SEM, XRD

Posted Date: February 12th, 2021

DOI: https://doi.org/10.21203/rs.3.rs-217328/v1

Version of Record: A version of this preprint was published at Journal of Inorganic and Organometallic Polymers and Materials on February 24th, 2021. See the published version at https://doi.org/10.1007/s10904-021-01947-w.

Effect of TiO_2 Nano-filler on Electrical Properties of Na^+ Ion Conducting PEO/PVDF Based Blended Polymer Electrolyte

Kiran Kumar Ganta[1], Venkata Ramana Jeedi[1], K. Vijaya Kumar[2], Yalla Mallaiah[3], E. Laxmi Narsaiah[1*]

[1]Department of Physics, B V Raju Institute of Technology, Narsapur, Medak, Telangana 502313, India.
[2]Department of Physics, JNTU Hyderabad, Kukatpally, Hyderabad, Telangana 500085, India.
[3]Department of Physics, University PG College, Secunderabad, Osmania University, Hyderabad, Telangana 500003, India

ABSTRACT

Nanocomposite Polymer Electrolyte (NCPE) films based on a blend of two polymers poly (ethylene oxide) (PEO) and poly (vinylidene fluoride) (PVDF) complexed with sodium perchlorate ($NaClO_4$) salt and Nano-filler Titanium dioxide (TiO_2) (i.e., (80wt%PEO/20wt%PVDF) + 7.5wt%$NaClO_4$+ xwt%TiO_2 where x = 3, 6, 9, 12, 15, and 18) were prepared and characterized as potential candidates for battery applications. Electrochemical Impedance Spectroscopy (EIS) has been employed between the frequencies 10 Hz and 4 MHz to investigate electrical, dielectric and electric modulus properties of the prepared NCPE films. Effect of TiO_2 Nano-filler concentration on the structural, ionic conductivity, and dielectric relaxation has been studied. The AC conductivity of the NCPE films at high frequencies obeys Jonscher's power law. The values of DC ionic conductivity calculated by fitting the AC conductivity spectra to the best fit of Joncher's power law are consistent with the values of DC ionic conductivity calculated from the bulk resistance (R_b) of the NCPE films. The ionic conductivity that depends on temperature follows the Arrhenius rule between the temperatures 298 K and 328 K. The maximum ionic conductivity at ambient temperature 8.75×10^{-5} S/cm was obtained for (80wt%PEO/20wt%PVDF) +7.5wt%$NaClO_4$ +15wt%TiO_2 NCPE film and it is attributed to the decrease in crystallinity. Using Wagner's polarization technique ionic transport numbers of various NCPE films were measured.

Keywords: TiO_2 Nano-filler, Electrochemical Impedance Spectroscopy, Ionic conductivity, SEM, XRD.

---

*Corresponding author
E-mail address: laxminarsaiah.emmadi@bvrit.ac.in (E. Laxmi Narsaiah)
ORCID: 0000-0001-9257-0067

1. Introduction

In the past decade, the rapid development of portable electrochemical devices based on portable computers, mobile phones, tablet computers, and notebook computers has attracted attention, which has increased the demand for high-energy batteries. Due to excellent cycle stability and high specific capacity, lithium ions are incorporated into the manufacture of commercially available batteries [1-5]. At the same time, lithium-ion batteries (LIBs) are relatively expensive and have safety restrictions due to their explosiveness. Therefore, out of concern for future technologies, we need rechargeable batteries that are low in toxicity, have significantly increased energy density, are easy to handle, are cost-effective and are safer than lithium. The huge expectations of the battery industry have led to the development of sodium batteries, whose performance characteristics are closer to those of lithium batteries [6-8]. Due to the chemical resemblance between lithium and sodium, many electrolytes used in the field of lithium batteries are usually also suitable for sodium-based batteries. H. K. Koduru et al. have studied dielectric and structural properties of PEO/PVP blended solid polymer electrolytes complexed with $NaIO_4$ salt and the highest room temperature conductivity 1.56 x 10^{-7} S/cm was obtained for the blend of polymers (65wt%PEO/25wt%PVP) complexed with 10wt%$NaIO_4$ salt [9]. G. Dave and D. K. Kanchan have reported highest ionic conductivity 2.81x10^{-7} S/cm at ambient temperature for the blend of polymers PEO/PAM (both polymers were taken in 1:1 ratio by weight) complexed with 17.5wt%$NaCF_3SO_3$ [10].

Solid Polymer Electrolytes (SPE) have important technical significance in manufacturing bulk electrochemical devices such as fuel cells, super-capacitors, batteries, smart windows, and sensing devices [11-15]. SPE materials are unique and have advantages over liquid electrolytes mainly associated with applications in batteries because of their attractive characteristics, such as lightweight, wide operating range of temperature, high energy density, long shelf life, no leakage, easy preparation, low toxicity, excellent stability during charge and discharge cycles, and considerable mechanical and thermal stability [16, 17]. So far, various solid polymer electrolytes have achieved the most advanced development, and their technical significance has been deeply moved by breakthroughs in energy storage devices such as batteries and super-capacitors [18-20]. However, the main limiting factor in SPEs is poor conductivity at ambient temperature. Various methods have been carried out to improve the ionic conductivity and mechanical strength of solid polymer electrolytes these include (i) blending of two polymers to prepare blended polymer electrolytes (BPE) [21-22] (ii) adding plasticizers to solid polymer electrolytes to prepare plasticized polymer electrolytes (PPE) [23,

24] (iii) adding inorganic Nano-fillers to prepare nanocomposite polymer electrolytes (NCPE) [25, 26]. The NCPE materials with Nano-fillers and polymer matrix have several useful properties, so they are considered as new functional materials. In addition, NCPE materials are becoming more and more important in the applications of ion-conducting nanocomposite solid polymer electrolytes [27], organic optoelectronic devices [28], and humidity sensing materials [29].

In the present study, we have chosen blend of poly (ethylene oxide) (PEO) and poly (vinylidene fluoride) (PVDF). The choice of the polymers to be blended plays an important role in obtaining good mechanical, thermal and electrical properties. Mahboube Mohamadi et al. reported the miscibility of blend of polymers PEO and PVDF [30]. PEO yields excellent performance due to its exceptional characteristics such as highly flexible ethylene oxide segments, high dielectric constant and the ability to dissolve different inorganic salts, so it is used for technical applications and is a good polymer for basic research [31, 32]. Due to the strong electron withdrawing functional group (-C-F), PVDF based SPEs have higher anode stability [33]. PVDF has a large dielectric constant and a lower dissipation factor. PVDF has been chosen as a co-polymer for this study because of its interesting electrochemical and mechanical properties [34]. Titanium dioxide (TiO_2) has been chosen as Nano-filler. Nano-fillers based on TiO_2 have several applications, such as volatile organic compound (VOC) sensors and self-heating sensors, because of its non-toxic and chemical stability properties [35-36]. Nanocomposite polymer electrolyte (NCPE) films were prepared with Sodium perchlorate ($NaClO_4$) salt and Titanium dioxide (TiO_2) Nano-filler using solution-cast technique. Various experimental techniques such as XRD and SEM have been employed to study the complexation and surface morphology of prepared NCPE films respectively. Electrochemical impedance spectroscopy (EIS) has been used at frequencies between 10 Hz and 4 MHz to study the electrical, dielectric and modulus properties of NCPE films in the temperature range of 298 K and 333 K. Wagner's polarization technique was used to measure ionic transport numbers of prepared NCPE films.

2. Experimental

2.1 Materials

Polymers PVDF (Avg. MW=2, 75,000 g/mol), PEO (Avg. MW=2, 00,000 g/mol), Nano-filler Titanium dioxide (TiO_2, particle size<50 nm) and salt Sodium perchlorate ($NaClO_4$, AR,

>=98.0%) were purchased from Sigma Aldrich. Common solvent N, N- Dimethylformamide, DMF (99.5%) was procured from MERCK.

2.2 Preparation of Nanocomposite polymer electrolyte (NCPE) films

The NCPE films (i.e., (80wt%PEO/20wt%PVDF)+ 7.5wt%$NaClO_4$ +xwt%TiO_2 (x=0, 3, 6, 9, 12, 15, and 18)) were prepared by traditional solution-casting method. Firstly, polymeric solution of the blend of polymers PEO and PVDF for compositional weight ratio (80wt%PEO/20wt%PVDF) was prepared by taking the amounts of PEO (2.4 g) and PVDF (0.6 g) in a beaker and dissolving them in the common solvent DMF (40 ml) at 60 °C with magnetic stirring for 2 h. Thereafter, 7.5wt% amount of $NaClO_4$ (0.225 g) and 3wt% amount of TiO_2 (0.09 g) with respect to the total amount of polymer blend (3 g) was added to polymeric solution and then the polymeric solution was again subjected to magnetic stirring for 36 h at room temperature for dissolution of the salt and Nano-filler to obtain clear viscous solution. Finally, this polymeric electrolyte viscous solution was casted onto glass petri-dish. For the film formation, the casted solution was kept in a temperature-controlled vacuum oven at 60 °C for 48 h and then cooled down to ambient temperature which resulted free-standing NCPE film. In the same way the NCPE films were prepared according to (80wt%PEO/20wt%PVDF) +7.5 wt%$NaClO_4$+xwt%TiO_2 (where x=3, 6, 9, 12, 15, and 18). The sample designations are listed in Table-1. All the NCPE films were stored in the desiccator. Fig. 1 shows the synthesis of NCPE films by solution casting method.

2.3 Characterization and impedance spectroscopic studies of NCPE films

The complexation of salt $NaClO_4$ and Nano-filler TiO_2 with the blend of polymers PEO/PVDF was investigated using Shimadzu XRD-7000 X-Ray Diffractometer between Bragg's angles 10° and 80°. The surface morphology of prepared NCPE films was analysed using Hitachi S-3700N Scanning Electron Microscope. The N4L-PSM1735 Impedance Analysis Interface was used in the frequency range from 100 Hz to 4 MHz to record the impedance spectra of prepared NCPE films. Impedance spectroscopy data were used to calculate the bulk resistance and to study the dielectric and electrical modulus properties of NCPE films. The DC ionic conductivity of NCPE films that depends on temperature was calculated between the temperatures 298 K and 333 K. Wagner's polarization technique was used to estimate the ionic transport number. The polarization was performed by applying a DC voltage of 2 V and the current was measured by a Digital Nano ammeter (Scientific Equipment Roorkee, Model DNM-121).

3. Results and Discussion

3.1 XRD studies

The XRD patterns of (80wt%PEO/20wt%PVDF) +7.5wt%$NaClO_4$ +xwt%TiO_2 (where x=0, 3, 6, 9, 12, 15 and 18) NCPE films are presented in Fig. 2. Two distinctive diffraction peaks at 19.24°, and 23.35° belonging to PEO which exhibits crystalline segment and these two maxima are attributed to the crystal planes (1 2 0) and (1 1 2) of the monoclinic crystal structure of PEO [9]. There are two significant low intensity peaks located at 20.53° and 36.32° in the NPCE films, which belong to the β phase and α phase of PVDF, respectively [37]. This confirms the polymorphism of PVDF [38]. The low intensity peaks at 25.17°, 27°, 37.75°, and 47.92° in the XRD pattern of NCPE films belong to TiO_2 [39]. The crystalline peaks at 22°, 25°, 32° and 36° pertaining to $NaClO_4$ [40] were not found in the NCPE films, which confirms that $NaClO_4$ is completely complexed in the blend of polymers PEO and PVDF.

3.2 SEM studies

The Scanning Electron Microscope (SEM) is commonly used to analyse the surface morphology of the NCPE films. The SEM images (1 kX magnification) of (80wt%PEO/20wt%PVDF) +7.5wt%$NaClO_4$ +xwt%TiO_2 NCPE films are shown in Fig. 3. The surface morphology and crystallinity of NCPE films play a significant role on the ionic conductivity. The NCPE film with smooth surface has better ionic conductivity [41]. The SEM micrographs of all the NCPE films show rough surface, consisting of several crystalline domains. From the Fig. 3 it can be observed that the NCPE-15 film has the smooth surface morphology. The morphology of the smooth surface of the NCPE-15 film is closely related to the decrease in the crystallinity of NCPE films [42] this helps the ionic transport in the polymer electrolyte, thereby increasing the ionic conductivity [43].

3.3 Conductivity studies

The effect of TiO_2 Nano-filler concentration (TiO_2 wt%) in NCPE films on the frequency-dependent conductivity (AC conductivity) between the temperatures 298 K and 338 K was studied. In the shorter frequency region, the conductivity values do not depend on the frequency, and the change in conductivity is due to the piling up of charge at the electrode-electrolyte interface and this produces a polarization effect. In the upper-frequency region, the conductivity rises swiftly with frequency. The well-known Jonscher's AC power law demonstrates the change in conductivity with frequency which is presented in the following expression

$$\sigma'(\omega) = \sigma_0 + A\omega^n$$

Here $\sigma'(\omega)$ is the conductivity at a particular frequency, σ_0 is the conductivity in the low frequency region, which does not depend on the frequency and known as DC conductivity, A is a constant, and n is the frequency-exponent and its value varies from 0 to 1. The DC ionic conductivity values were calculated by fitting the graph to the best fit of Jonscher's power law using the origin 8.5 program. The calculated values were designated as $\sigma_{dc\ (power\ law)}$ and the values were reported in Table-1. Fig. 4 shows the frequency-dependent AC conductivity (σ') of prepared NCPE films at room temperature. Dotted lines represent Jonscher's power law fit in consistent with the experimental data.

DC ionic conductivity can also be calculated from complex impedance plot by taking bulk resistance (R_b) of the NCPE films. The conventional impedance spectroscopy technique involves measuring the impedance (Z) of NCPE film as a function of frequency $f\ (\omega = 2\pi f)$ over a wide frequency range, and plotting $Z(f)$ against frequency in the form of $Z''(f)$ against $Z'(f)$ for various frequencies. The resulting graph is called a complex impedance plot. Sometimes the plot is called the Nyquist plot, which is strictly applicable to electronic circuits. Such diagrams can be used to evaluate the electrical parameters of the system under study. For impedance study, the NCPE film is sandwiched between two electrodes, allowing ions to penetrate the electrodes. Such electrodes are called non-blocking electrodes. Generally, since any NCPE film can show resistance and capacitance characteristics, it can be regarded as a combination of resistors and capacitors connected in parallel [44-45]. Fig. 5a shows the complex impedance plot for various NCPE films at ambient temperature and equivalent circuit of NCPE film. Fig. 5b shows the complex impedance plot for NCPE-15 film at different temperatures. From Fig. 5a it can be observed that NCPE-15 film has the lowest bulk resistance (R_b), so it has the highest ionic conductivity at ambient temperature. The complex impedance plot shows the semicircle of the NCPE-15 film at all temperatures, indicating that the sample is partially capacitive and resistive. Similar behavior could be observed for all remaining NCPE films as well. The obtained complex impedance plots were fitted in circles using origin8.5 program. The intercept of a fitted circle on the real Z-axis (Z') is used to obtain the bulk resistance (R_b) of the NCPE film [46-48]. The values of DC ionic conductivities of various prepared NCPE films were determined using the relation, $\sigma_{dc} = \frac{t}{AR_b}$ where t is the thickness, A is the area of cross section and R_b is the bulk resistance of the NCPE film. The DC ionic conductivity values calculated using Jonscher's power law are consistent with the values

calculated from the bulk resistance. The DC ionic conductivity values calculated from the bulk resistance and designated, as $\sigma_{dc(Rb)}$ which were reported in Table-1.

Fig. 6 shows the temperature-dependent ionic conductivities of various prepared NCPE films. The temperature-dependent ionic conductivity of all NCPE films follow the Arrhenius rule in the temperature range from 298 K to 328 K. It can be observed from the Fig. 6 that the NCPE-15 film yields good ionic conductivity results and hence, it is the optimum conducting composition (OCC) for the system under investigation. The highest ionic conductivity 8.75 x10^{-5} S/cm was obtained for NCPE-15 film at room temperature and ionic conductivity values of other polymer electrolyte systems reported in the past literature are compared in Table-2.

The ionic transport numbers of various prepared NCPE films were calculated using Wagner's polarization technique. The NCPE film was polarized under constant DC voltage of 2V and measured the current values with respect to time. The initial current (i_i) is the total current of NCPE films, which is due to the electrons and ions. As the polarization rises, the current is blocked due to the ions and the final current (i_f) is due to the electrons. The initial current decreases with time due to the reduction of ionic species in the NCPE films and becomes constant. At this stage, the final current is due to electrons only. The ionic transport numbers of NCPE films were measured by the following expression

$t_i = \frac{i_i - i_f}{i_i}$ and the electronic transport number $t_e = 1 - t_i$

The values of ionic transport numbers are listed in Table-1.

3.4 Dielectric studies

The dielectric constant of a material is the property used to measure the energy it stores. The following relation gives the frequency-dependent complex dielectric function (ε^*) of SPE films

$$\varepsilon^* = \varepsilon'(\omega) - i\varepsilon''(\omega) = \frac{1}{i\omega C_0 Z^*}$$

where ε' and ε'' are the real and imaginary parts of the complex permittivity respectively, C_0 is the capacitance of the material in vacuum, ω is the angular frequency, and Z^* is the complex impedance. The values of ε' and ε'' were taken from electrochemical impedance spectroscopic data. Fig. 7 shows the real parts of complex permittivity of (80wt%PEO/20wt%PVDF) +7.5wt% $NaClO_4$ + xwt%TiO_2 NCPE films at room temperature and NCPE-15 film at different temperatures respectively.

Fig. 8 shows the imaginary parts of complex permittivity of (80wt%PEO/20wt%PVDF) +7.5wt%$NaClO_4$ +xwt%TiO_2 NCPE films at room temperature and NCPE-15 film at different temperatures respectively. From the Fig. 7a and Fig. 8a it can be observed that NCPE-15 film has the maximum values of ε' and ε'' and both ε' and ε'' show the analogous behaviour with frequency at various temperatures. As frequency increases ε' deceases and reaches saturation at upper frequencies. The value of the dielectric constant is higher at low frequencies, which is because of the orientation of the ions, polar groups and space charge polarization near the electrodes. In contrast, the dielectric constant is lower at high frequencies due to dielectric relaxation [49-52]. There are no relaxation maxima in both ε' and ε'', indicating that the rise in ionic conductivity is primarily because of increased mobile ions.

Fig. 9 shows the tangent loss of (80wt%PEO/20wt%PVDF) +7.5wt%$NaClO_4$ +xwt%TiO_2 NCPE films at room temperature and NCPE-15 film at different temperatures respectively. Energy dissipation due to charge transfer and electrode polarization effects can be measured by dielectric loss. From the Fig. 9, it can be observed that the loss tangent ($\tan\delta = \varepsilon''/\varepsilon'$) is proportional to frequency and reaches a peak at a specific characteristic frequency. After reaching the peak value, the $\tan\delta$ value decreases with an increase in frequency. As the temperature rises, the peak moves to the right [53]. The peaks obtained at particular frequencies are due to the polarization of the electrode. If f is the frequency related to the relaxation peak, then the relaxation time (τ) is specified as $\tau = 1/2\pi f$. Therefore, as the relaxation time decreases, the ionic conductivity increases [54].

From Fig. 9a, it can be observed that NCPE-15 film has the highest relaxation peak among all the prepared NCPE films, and it has the highest ionic conductivity. At higher temperatures, because of heat generation defects in the polymer electrolyte, the relaxation time decreased, and a higher conductivity was obtained, which is consistent with Arrhenius behavior.

3.5 Electric modulus studies

The dominant low-frequency electrode interface polarization arrests all other relaxation mechanisms. Therefore, it is necessary to use the formulation of electric modulus spectroscopy to study the dielectric properties further to suppress the influence of mobile ion polarization or electrode polarization. Many researchers have studied electrical modulus to analyse and understand electrical relaxation data in various materials. This formalism provides broad insights into the process of charge transport, such as ionic dynamics and the relaxation mechanism of conductivity with temperature and frequency [55, 56].

The electric modulus M^* and complex dielectric permittivity ε^* in the electric modulus formalism are related as

$$M^* = {}^{1}/_{\varepsilon^*} = (\varepsilon' - j\varepsilon'')/|\varepsilon^*|^2 = M' + jM''$$

where M' and M'' are the real and imaginary parts of the complex modulus M^* respectively.

Fig. 10 shows the real parts of electric modulus spectra of (80wt%PEO/20wt%PVDF) +7.5wt% $NaClO_4$ + xwt%TiO_2 NCPE films at room temperature and NCPE-15 film at different temperatures respectively.

Fig. 11 shows the imaginary parts of electric modulus spectra of (80wt%PEO/20wt%PVDF) +7.5wt% $NaClO_4$ + xwt%TiO_2 NCPE films at room temperature and NCPE-15 film at different temperatures respectively. From the Fig. 10 it can be observed that M' shows an excellent dispersion with increasing frequency, and tends to attain high constant value at higher frequencies. It can be seen from Fig. 11 that M'' shows a relaxation peak. The lower value of M'in the low frequency region allows ion conduction movement, while M'' shows a relaxation peak, which confirms the ionic nature of the NCPE film. The peak indicates ionic conductivity relaxation of the sodium ions in the system. The lower frequency side of the maximum suggests the long-range movement of charge carriers, while the higher frequency side of the maximum refers to the cage motion of moving ions. The movement of charge carriers receives a gain with increasing temperature. This results in lower relaxation time, and as a result, the peak value of M'' shifts towards higher frequencies [57, 58]. This type of change recommends that relaxation is thermally activated and charge carrier hopping takes place.

4 Conclusions

Nanocomposite Polymer Electrolyte (NCPE) films of (80wt%PEO/20wt%PVDF) + 7.5wt% $NaClO_4$ + xwt%TiO_2; where x = 3, 6, 9, 12, 15, and 18) were synthesized using solution-cast technique. The effect of TiO_2 Nano-filler concentration on the structural, morphological, ionic conduction and dielectric polarization was studied. The XRD patterns of the NCPE films confirm that the $NaClO_4$ salt and TiO_2 Nano-filler were totally dissolved in the NCPE films. SEM studies show that the NCPE-15 film has smooth surface morphology, which is directly correlated to the decrease of crystallinity and an increase in the amorphous region. The DC ionic conductivity follows the Arrhenius rule between the temperatures 303 K and 373 K. The NCPE-15 film has the highest ionic conductivity 8.75×10^{-5} S/cm at room temperature and it is

attributed to the decrease in crystallinity. From the transport number measurements, it can be observed that majority contribution is ionic, which will be good for battery shelf life.

Acknowledgement

The authors sincerely thank the management of B V Raju Institute of Technology (BVRIT-N), Narsapur for continuous support.

Funding

The Jawaharlal Nehru Technological University Hyderabad (JNTUH), India, financially supported this work under grant JNTUH/TEQIP-III/CRS/2019/Physics/04.

Declaration of interest statement

The authors have no conflicts of interest to declare that are relevant to the content of this article.

The authors have no relevant financial or non-financial interests to disclose.

References

1. Y. Yamada, Bull. Chem Soc Jpn. (2020) https://dx.doi.org/10.1246/bcsj.20190314
2. F.J. Sonia, M. Aslam, A. Mukhopadhyay, Carbon. (2020) https://doi.org/10.1016/j.carbon.2019.09.026
3. J. M. Tarascon, M. Armand, Nature. (2001) https://doi.org/10.1038/35104644
4. D. Zhang, R. Li, T. Huang, A. Yu, J power sources. (2010) https://doi.org/10.1016/j.jpowsour.2009.08.063
5. J.A. Lee, J.Y. Lee, M.H. Ryou, G.B. Han, J.N. Lee, D.J. Lee, J.K. Park, Y.M. Lee, J Solid State Electrochem. (2011) https://doi.org/10.1007/s10008-010-1149-y
6. V. Palomares, P. Serras, I. Villaluenga, K.B. Hueso, J. Carretero-Gonzalez, T. Rojo, Energy Environ Sci. (2012) https://doi.org/10.1039/C2EE02781J
7. H.K.Koduru, Y.G.Marinov, G.B.Hadjichristov, N.Scaramuzza, Solid State Ionics. (2019) https://doi.org/10.1016/j.ssi.2019.02.021
8. L. Wang, Y. Lu, J. Liu, M. Xu, J. Cheng, D. Zhang, J.B. Goodenough, Angewandte Chemie. (2013) https://doi.org/10.1002/anie.201206854
9. H.K. Koduru, L. Marino, F. Scarpelli, A.G. Petrov, Y.G. Marinov, G.B. Hadjichristov, M.T. Iliev, N. Scaramuzza, Curr Appl Phys. (2017) https://doi.org/10.1016/j.cap.2017.07.012
10. G. Dave, D. K. Kanchan, Indian J. pure Appl. Phys. 56, 978 (2018)

11. K.M. Anilkumar, B. Jinisha, M. Manoj, S. Jayalekshmi, Eur Polym J. (2017) https://doi.org/10.1016/j.eurpolymj.2017.02.004
12. Nidhi, S. Patel, R. Kumar, J Alloy Compd. (2019) https://doi.org/10.1016/j.jallcom.2019.03.089
13. K. Murata, Electrochimica Acta. (1995) https://doi.org/10.1016/0013-4686(95)00160-G
14. A. Chandra, A. Chandra, K. Thakur, Chin J Polym Sci. (2013) https://doi.org/10.1007/s10118-013-1223-x
15. H.W. Zhang, P.K. Shen, Chem Rev. (2012) https://doi.org/10.1021/cr200035s
16. Y. Kato, S. Hori, T. Saito, K. Suzuki, M. Hirayama, A. Mitsui, M. Yonemura, H. Iba, R. Kanno, Nat Energy. (2016) https://doi.org/10.1038/nenergy.2016.30
17. J. Li, C. Ma, M. Chi, C. Liang, N.J. Dudney, Adv Energy Mater. (2015) https://doi.org/10.1002/aenm.201401408
18. L. Yue, J. Ma, J. Zhang, J. Zhao, S. Dong, Z. Liu, G. Cui, L. Chen, Energy Storage Mater. (2016) https://doi.org/10.1016/j.ensm.2016.07.003
19. Q. Zhang, K. Liu, F. Ding, X. Liu, Nano Res. (2017) https://doi.org/10.1007/s12274-017-1763-4
20. Gracia, M. Armand, D. Shanmukaraj, Solid Electrolytes for Advanced Applications, (Springer, Cham, 2019), pp. 347-373
21. F.H. Abd El-kader, N.A. Hakeem, R.S. Hafez, A.M. Ismail, J Inorg Organomet Polym Mater. (2017) https://doi.org/10.1007/s10904-017-0763-x
22. D.W. Kim, J.K. Park, H.W. Rhee HW, Solid State Ionics. (1996) https://doi.org/10.1016/0167-2738(95)00238-3
23. P. Dhatarwal, R.J. Sengwa, Indian J Pure Appl Phys. 55,7 (2017)
24. S. Das, A. Ghosh, Electrochimica Acta. (2015) https://doi.org/10.1016/j.electacta.2015.04.178
25. Y.L. Nimah, M.Y. Cheng, J.H. Cheng, J.Rick, B.J. Hwang, J Power Sources. (2015) https://doi.org/10.1016/j.jpowsour.2014.11.047
26. M.A.K.L. Dissanayake, Ionics. (2004) https://doi.org/10.1007/BF02382820
27. S. Choudhary, R. J. Sengwa, J Inorg Organomet Polym Mater. (2019) https://doi.org/10.1007/s10904-018-1034-1
28. T.P. Nguyen, Surf Coat Technol. (2011) https://doi.org/10.1016/j.surfcoat.2011.07.010

29. A. Hashim, Q. Hadi, J Inorg Organomet Polym Mater. (2018) https://doi.org/10.1007/s10904-018-0837-4
30. M. Mohamadi, H. Garmabi, M. Papila, Macromolecular Res. (2016) https://doi.org/10.1007/s13233-016-4099-0
31. K. Xu, Chem Rev. (2014) https://doi.org/10.1021/cr500003w
32. E. Quartarone, P. Mustarelli, Chem Soc Rev. (2011) https://doi.org/10.1039/C0CS00081G
33. H.S. Choe, J. Giaccai, M. Alamgir, K.M. Abraham, Elecrochimica Acta. (1995) https://doi.org/10.1016/0013-4686(95)00180-M
34. F. Croce, G.B. Appetecchi, S. Slane, M. Salomon, M. Tavarez, S. Arumugam, Y. Wang, S.G. Reenbaum, Solid State Ionics. (1996) https://doi.org/10.1016/0167-2738(96)00137-3
35. A. Ramanavicius, P. Genys, Y. Oztekin, A. Ramanaviciene, J. Electrochemical Society. (2014) https://doi.org/10.1149/2.021403jes
36. A. Ramanavicius, P. Genys, A. Ramanaviciene, Elecrochimica Acta. (2014) https://doi.org/10.1016/j.electacta.2014.08.130
37. A.M. Gaur, D.S. Rana, J Inorg Organomet Polym Mater. (2019) https://doi.org/10.1007/s10904-019-01126-y
38. P. Dhatarwal, R.J. Sengwa, Macromol Res. (2019) https://doi.org/10.1007/s13233-019-7142-0
39. R.J. Sengwa, S. Choudhary, P. Dhatarwal, J Mater Sci. (2019) https://doi.org/10.1007/s10854-019-01587-4
40. K.K. Ganta, V.R. Jeedi, K.V. Kumar, E.L. Narsaiah, J Green Engineering. 10, 5589 (2020)
41. N. Angulakshmi, D.J. Yoo, K.S. Nahm, C. Gerbaldi, A.M. Stephan, Ionics. (2013) https://doi.org/10.1007/s11581-013-0985-z
42. P. Prabakaran, R.P. Manimuthu, S. Gurusamy, J Solid State Electrochem. (2016) https://doi.org/10.1007/s10008-016-3477-z
43. N.K. Singh, M.L. Verma, M. Minakshi, Bull Mater Sci. (2015) https://doi.org/10.1007/s12034-015-0980-2
44. A. Ramanavicius, P. Genys, Y. Oztekin, A. Ramanaviciene, J Electrochemical Society. (2014) https://doi.org/10.1149/2.021403jes
45. A. Ramanavicius, P. Genys, A. Ramanaviciene, Elecrochimica Acta. (2014) https://doi.org/10.1016/j.electacta.2014.08.130

46. E. Barsoukov, J.R. Macdonald, Impedance Spectroscopy: Theory, Experiment, and Applications, 2nd edn. (John Wiley & Sons, Hoboken, New Jersey, 2015), pp. 616
47. S.B. Aziz, T.J. Woo, M.F.Z. Kadir, H.M. Ahmed, J Science: Advanced Mater Devices. (2018) https://doi.org/10.1016/j.jsamd.2018.01.002
48. D. Vanitha, S. A. Bahadur, N. Nallamuthu, S. Athimoolam, A. Manikandan, J Inorg Organomet Polym Mater. (2016) https://doi.org/10.1007/s10904-016-0468-6
49. I.M. Hodge, M.D. Ingram, A.R. West, J Electroanal Chem. (1976) https://doi.org/10.1016/S0022-0728(76)80229-X
50. S.R. Majid, A.K. Arof, Phys B: Condensed Matter. (2007). https://doi.org/10.1016/j.physb.2006.08.038
51. R. Manjuladevi, M. Thamilselvan, S. Selvasekarapandian, R. Mangalam, M. Premalatha, S. Monisha, Solid State Ionics. (2017) http://dx.doi.org/10.1016/j.ssi.2017.06.002
52. R.S. Hafez, N.A. Hakeem, A.A. Ward, A.M. Ismail, F.H. Abd El-kader, J Inorg Organomet Polym Mater (2020) https://doi.org/10.1007/s10904-020-01637-z
53. V.R. Jeedi, E.L. Narsaiah, M. Yalla, R. Swarnalatha, S.N. Reddy, A.S. Chary, SN Appl Sci. (2020) https://doi.org/10.1007/s42452-020-03868-8
54. S. Choudhary, R.J. Sengwa, Indian J Pure Appl Phys. 49:204 (2011)
55. A. Karmakar, A. Ghosh, Curr Appl Phys. (2012) https://doi.org/10.1016/j.cap.2011.08.017
56. R.J. Sengwa, P. Dhatarwal, S. Choudhary, Solid State Ionics. (2018) https://doi.org/10.1016/j.ssi.2018.07.015
57. K.K. Ganta, V.R. Jeedi, K.V. Kumar, E.L. Narsaiah, Int J Polym Anal Characterization. (2020) https://doi.org/10.1080/1023666X.2020.1860396
58. P. Pal, A. Ghosh, Solid State Ionics. (2018) https://doi.org/10.1016/j.ssi.2018.02.009
59. K. Sundaramahalingam, M. Muthuvinayagam, N. Nallamuthu, Polym Sci Ser A. (2019) https://doi.org/10.1134/S0965545X19050171
60. S. K. Shahenoor Basha, G. S. Sundari, K. V. Kumar, M. C. Rao, Polym Bull. (2018) https://doi.org/10.1007/s00289-017-2072-5

Figures

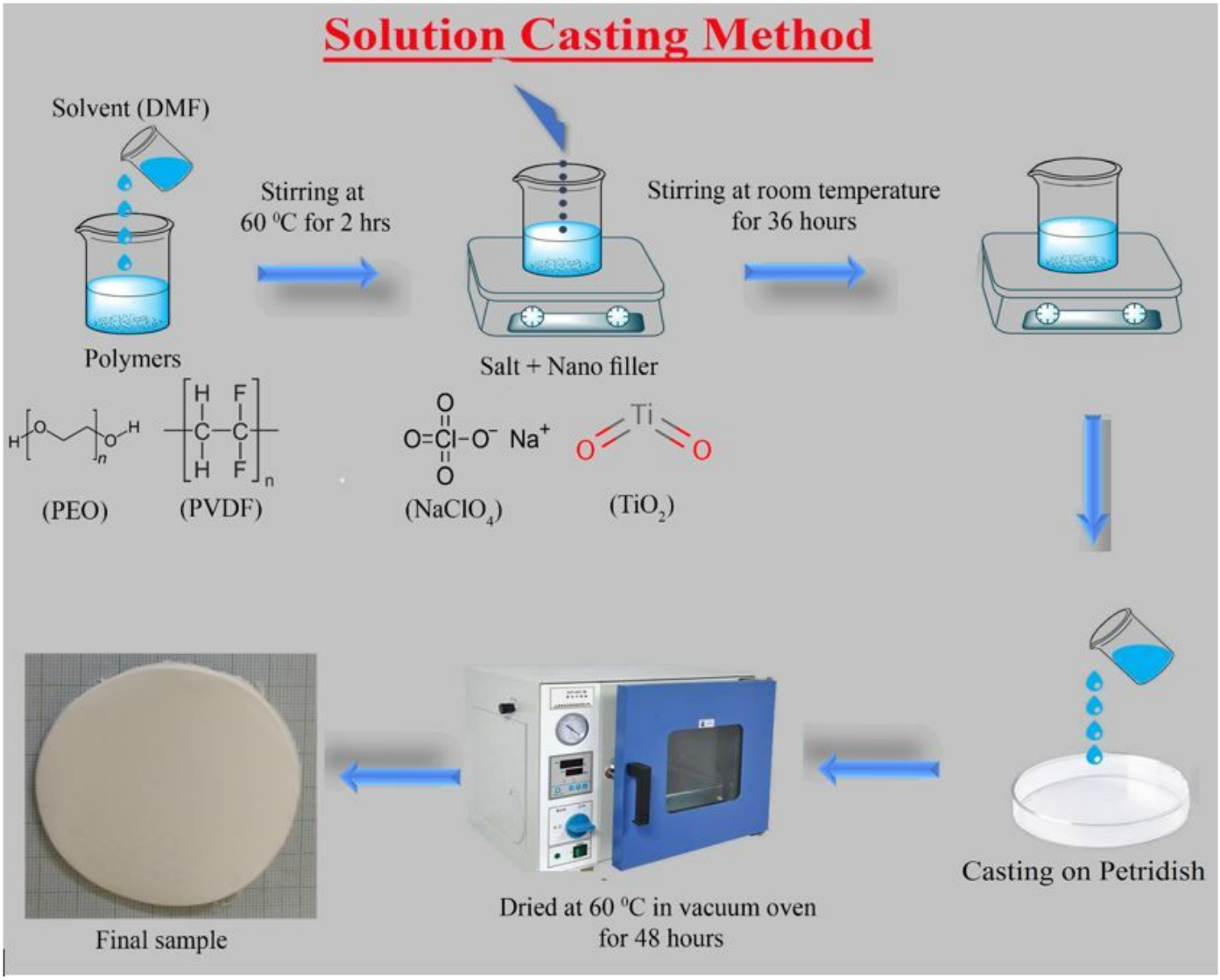

Figure 1

Solution Casting Method

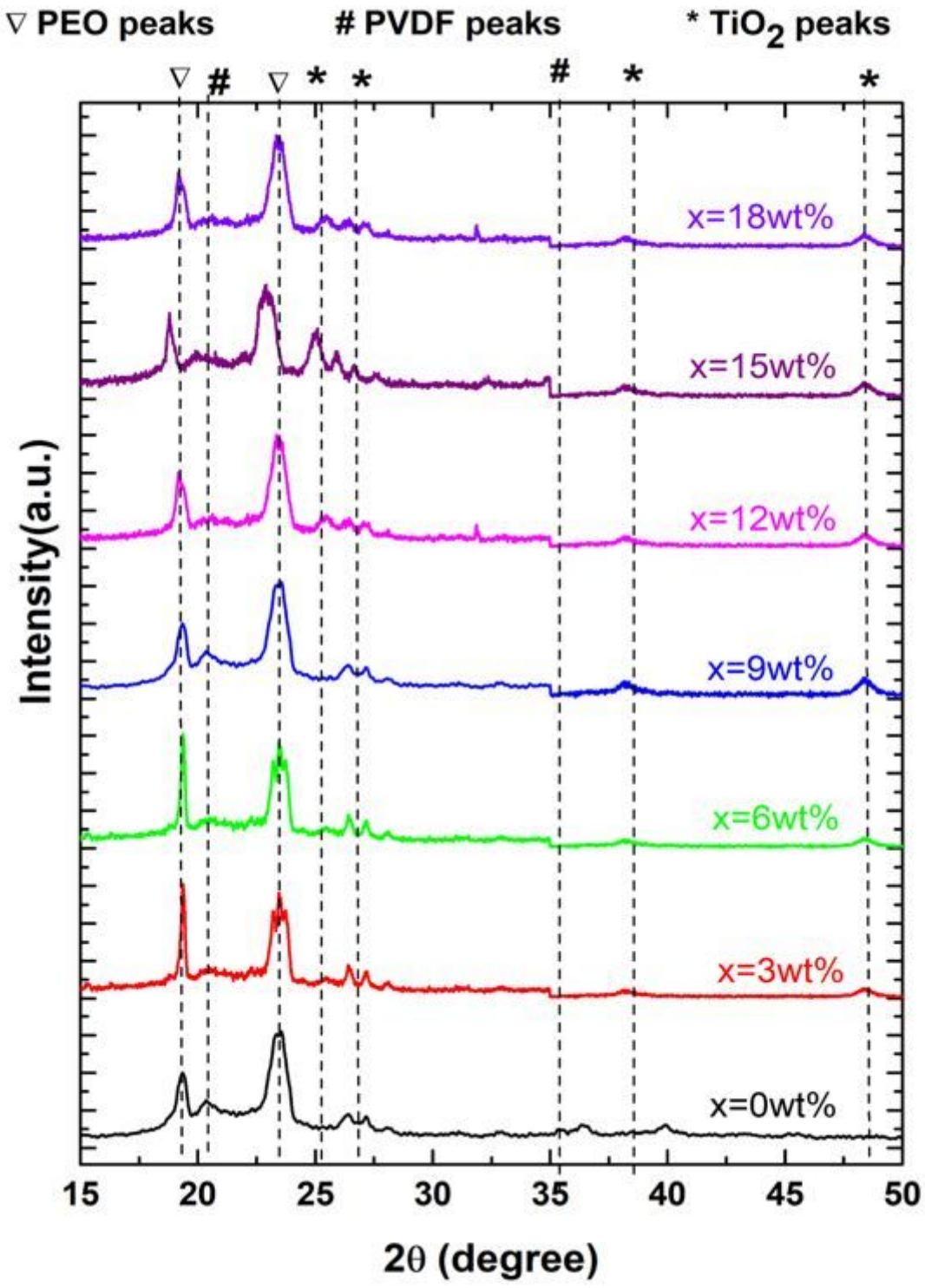

Figure 2

XRD patterns of (80wt%PEO/20wt%PVDF) +7.5wt%NaClO4 +xwt%TiO2 NCPE films

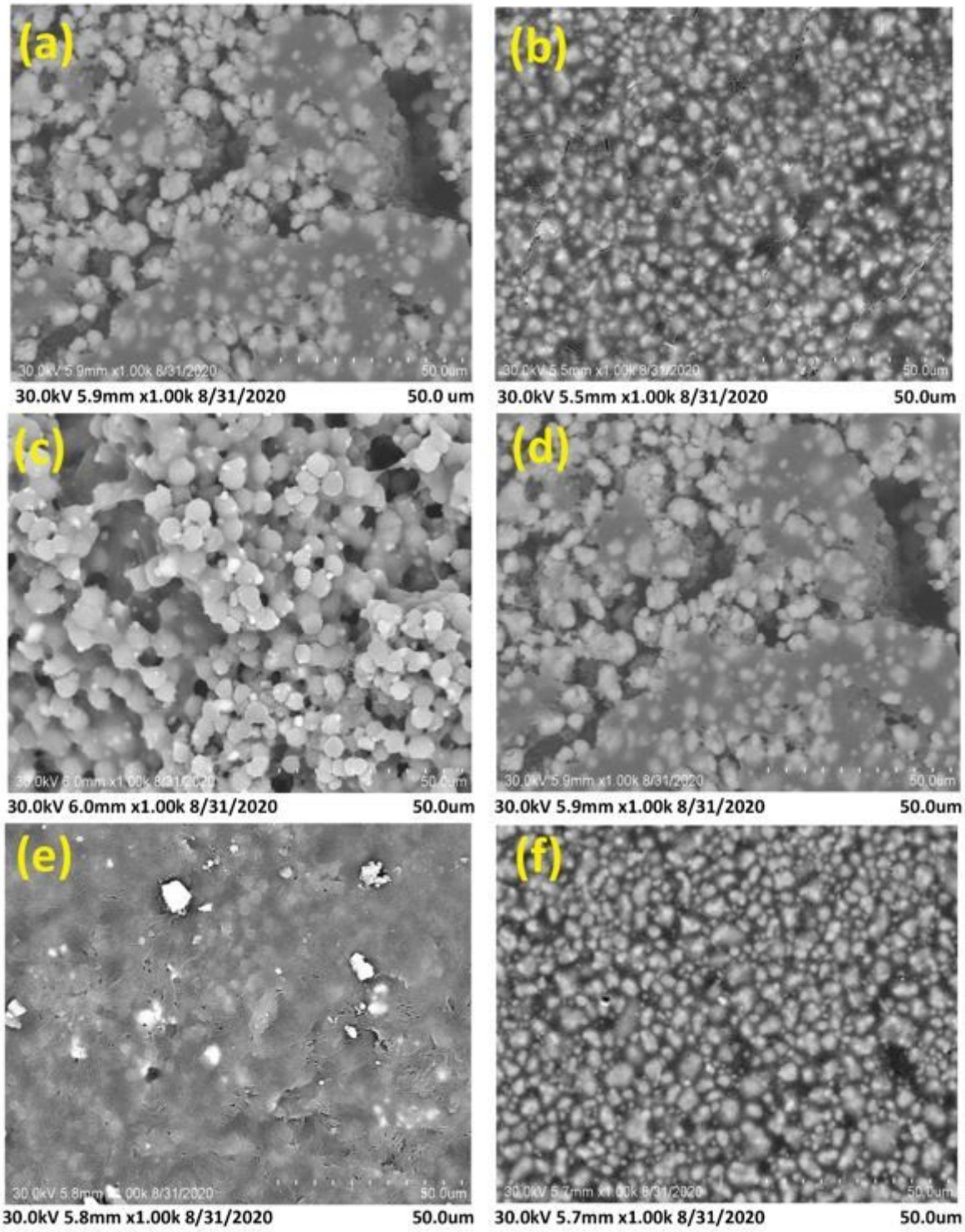

Figure 3

SEM images of (80wt%PEO/20wt%PVDF) +7.5wt%NaClO4 +xwt%TiO2 NCPE films (a) x =3 (b) x = 6 (c) x = 9 (d) x =12 (e) x=15 and (f) x=18

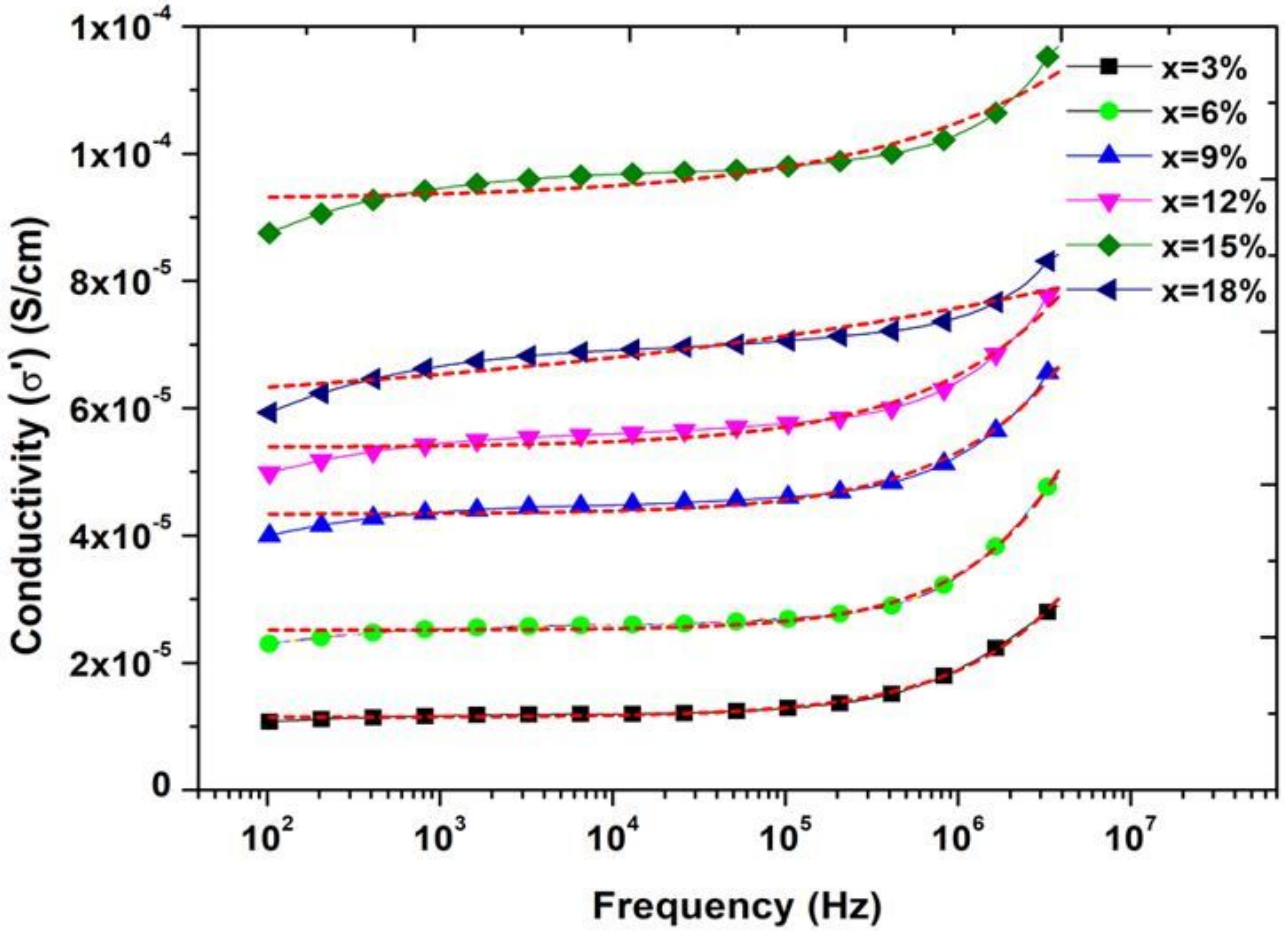

Figure 4

Frequency-dependent AC conductivity (σ^') of (80wt%PEO/20wt%PVDF) +7.5wt%NaClO4 +xwt%TiO2 NCPE films at room temperature. Dotted lines represent the Jonscher's power law fit of the experimental data

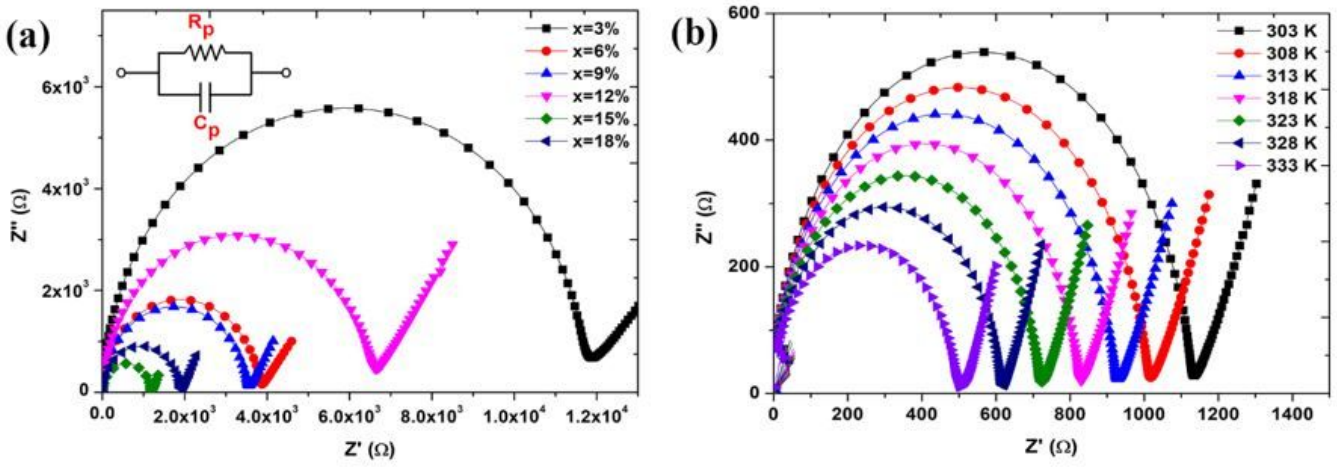

Figure 5

a Complex impedance plot of (80wt%PEO/20wt%PVDF) +7.5wt%NaClO4 + xwt%TiO2 NCPE films at room temperature b Complex impedance plot of NCPE-15 film at different temperatures.

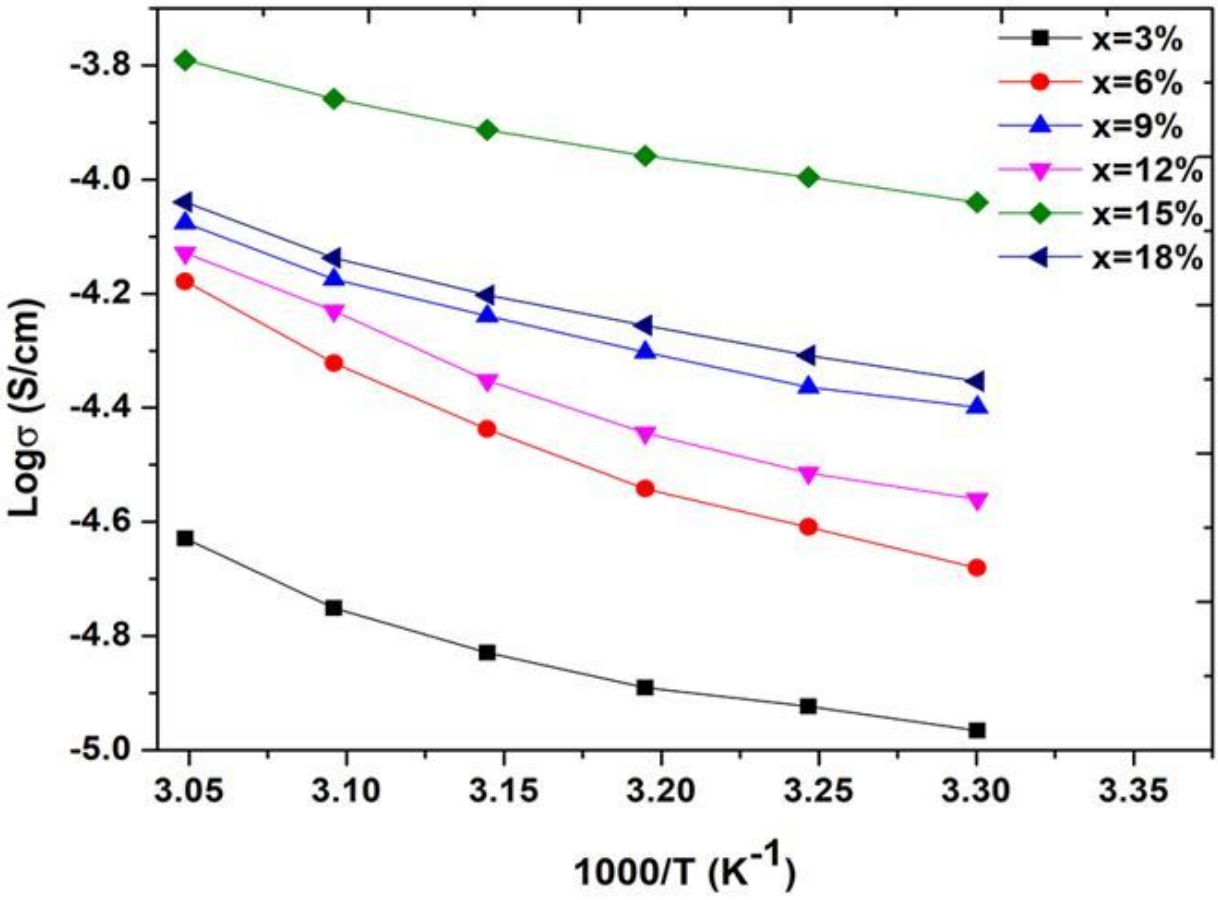

Figure 6

Temperature-dependent ionic conductivity of (80PEO/20PVDF) +7.5wt% NaClO4 + xwt%TiO2 NCPE films between the temperatures 298 K and 328 K

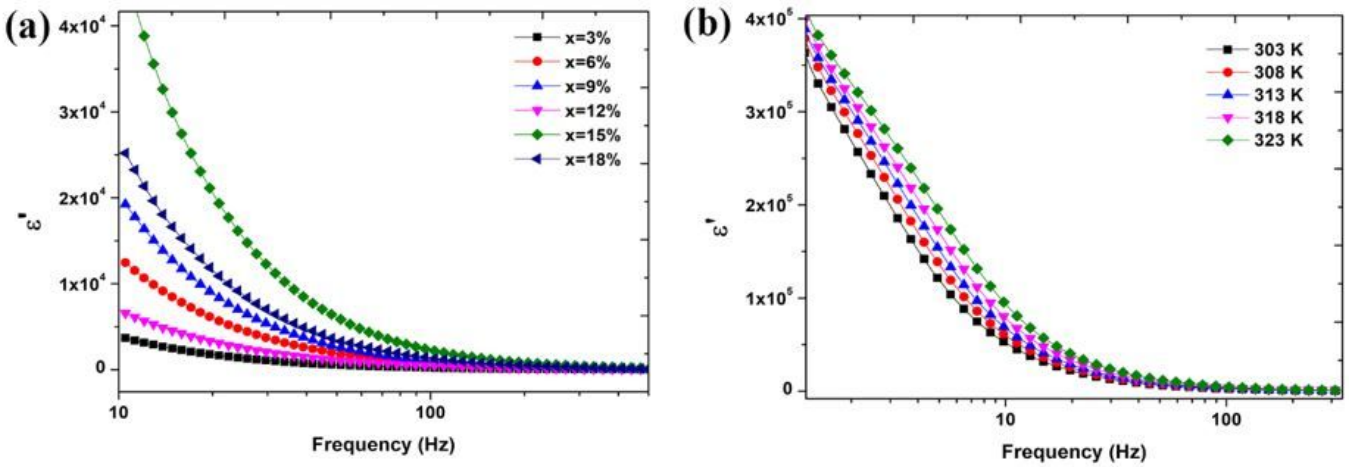

Figure 7

a The real parts of complex permittivity of (80PEO/20PVDF) +7.5wt% NaClO4 + x wt%TiO2 NCPE films at room temperature b The real parts of complex permittivity of NCPE-15 film at different temperatures.

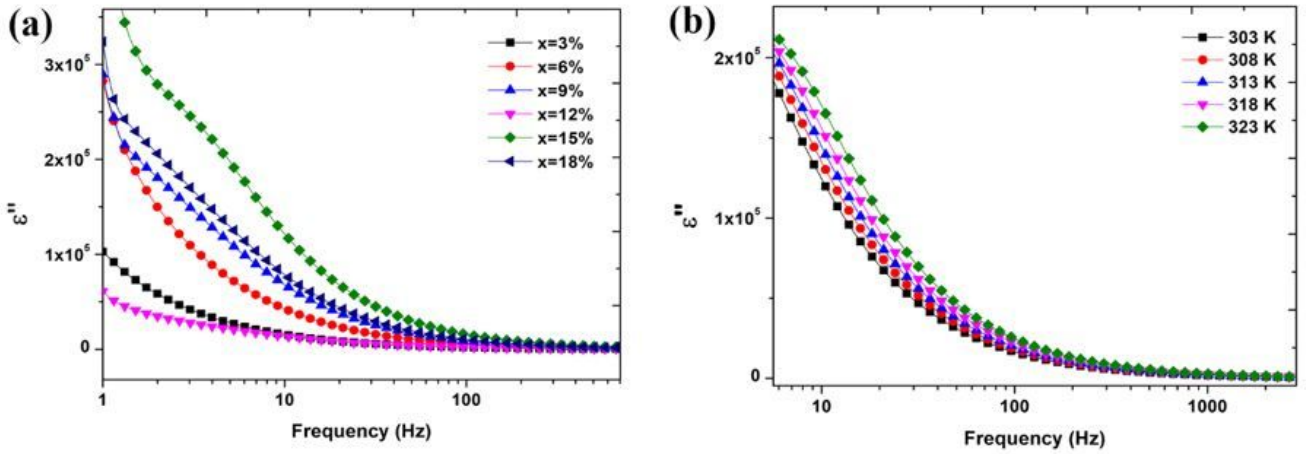

Figure 8

a The imaginary parts of complex permittivity of (80PEO/20PVDF) +7.5wt% NaClO4 + xwt%TiO2 NCPE films at room temperature b The imaginary parts of complex permittivity of NCPE-15 film at different temperatures.

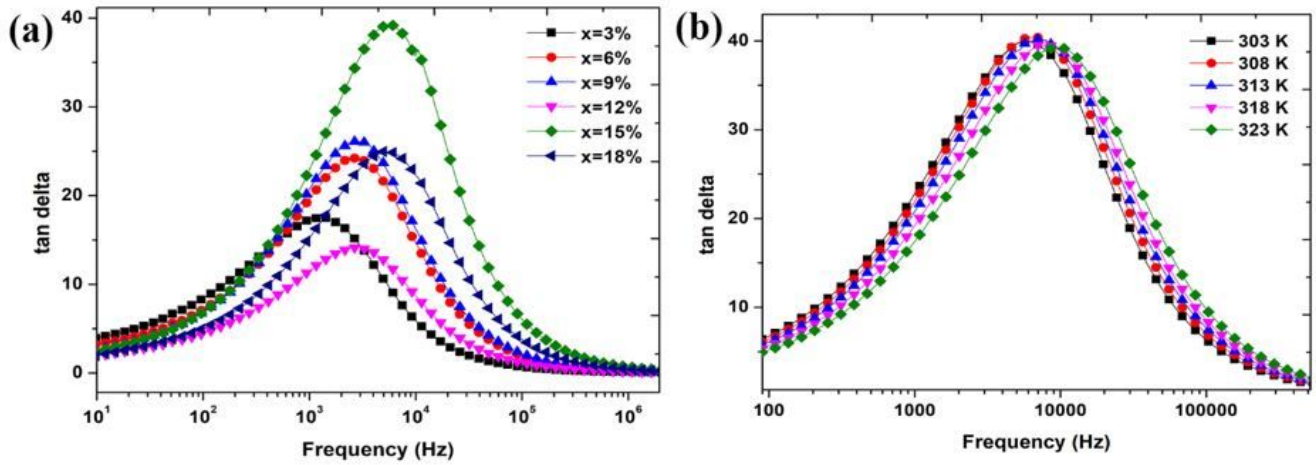

Figure 9

a Tangent loss of (80PEO/20PVDF) +7.5wt%NaClO4 +xwt%TiO2 NCPE films at room temperature b Tangent loss of NCPE-15 film at different temperatures.

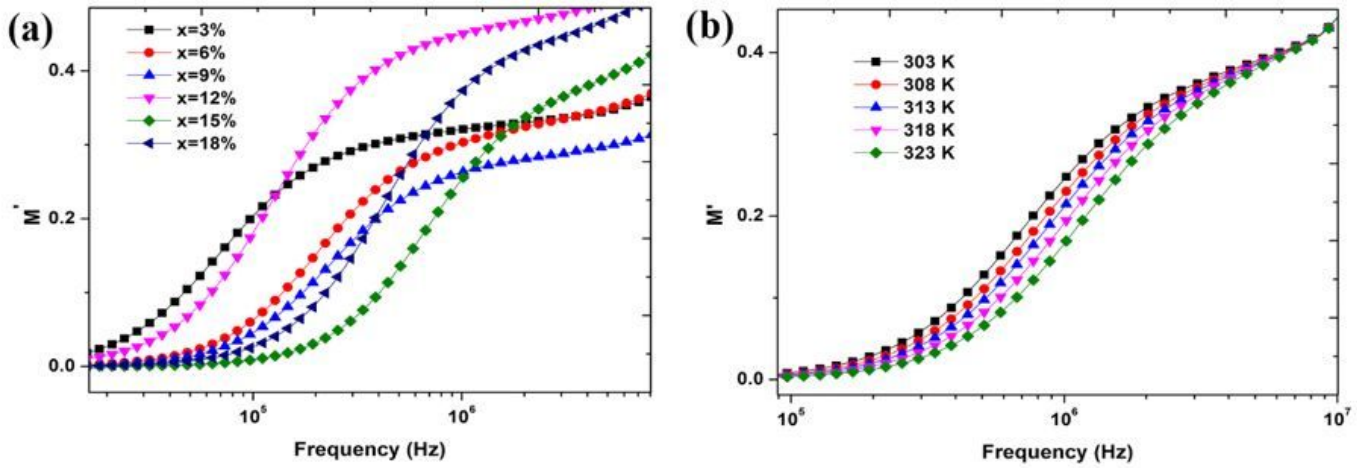

Figure 10

a The real parts of electric modulus spectra of (80PEO/20PVDF) +7.5wt% NaClO4 + xwt%TiO2 NCPE films at room temperature b The real parts of electric modulus spectra NCPE-15 film at different temperatures

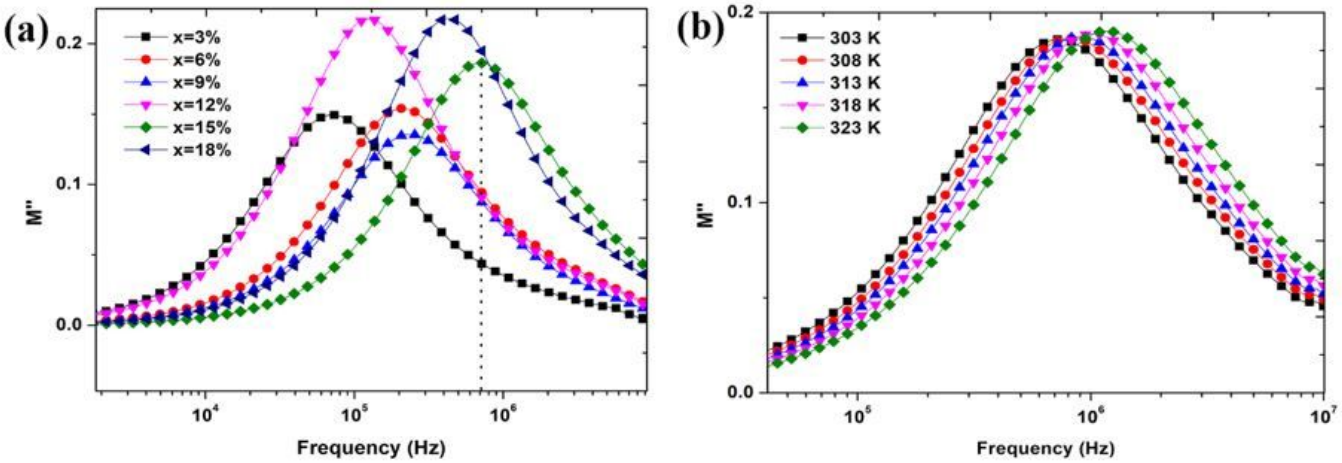

Figure 11

a The imaginary parts of electric modulus spectra of (80PEO/20PVDF) +7.5wt% NaClO4 + xwt%TiO2 NCPE films at room temperature b The imaginary parts of electric modulus spectra of NCPE-15 film at different temperatures